

Measurement of hydrogen in alloys by magnetic and electronic techniques

P. Termsuksawad^a, S. Niyomsoan^a, R.B. Goldfarb^b, V.I. Kaydanov^a,
D.L. Olson^{a,*}, B. Mishra^a, Z. Gavra^c

^a Colorado School of Mines, Golden, CO 80401, USA

^b National Institute of Standards and Technology, Boulder, CO 80305, USA

^c Nuclear Research Center - Negev, Beer Sheva 84190, Israel

Received 28 May 2003; received in revised form 13 October 2003; accepted 14 October 2003

Abstract

As demonstrated in this paper, magnetic and electronic measurements can be used to quantify hydrogen availability, absorption, and desorption in materials for nickel metal-hydride batteries and hydrogen storage. The ability of a metal alloy to absorb and desorb hydrogen depends on the interaction of the metal's electronic bands with electrons donated or accepted by the hydrogen. The tendency of alloys to dissolve hydrogen and form hydrides depends on their performance as electron acceptors. Absorbed hydrogen may exist in either soluble (protonic) or bound phases. Magnetization and thermoelectric (Seebeck) coefficient were measured as functions of hydrogen content in powdered AB₅- and AB₂-type alloys. Magnetization decreases with increasing soluble hydrogen in ferromagnetic AB₅-type (La–Ce)(Ni–Mn)₅ and (La–Nd)(Ni–Co–Mn)₅. However, magnetization *increases* with increasing soluble hydrogen in AB₂-type (Zr–Ti)(Cr–Fe)₂. Finally, magnetization does not change with increasing *bound* hydrogen in AB₂-type (Zr–Ti)(Ni–Mn–Cr–V)₂. The Seebeck coefficient for AB₅-type (La–Nd)(Ni–Co–Mn)₅ is a monotonically decreasing function of hydrogen content. However, the effect of absorbed hydrogen on the Seebeck coefficient of the AB₂ alloys depends on whether the hydrogen is soluble or bound.

© 2003 Elsevier B.V. All rights reserved.

Keywords: Hydrogen storage materials; Gas–solid reactions; Electronic band structure; Electronic transport; Magnetic measurements

1. Introduction

Rare-earth transition-metal alloys, such as LaCo₅ and LaNi₅ have long been studied as candidate materials for metal-hydride batteries and hydrogen storage devices [1]. In rechargeable nickel metal-hydride (NiMH) batteries, nickel is the positive electrode (anode) and a metal alloy with absorbed hydrogen is the negative electrode (cathode). In this cell, potassium hydroxide is the electrolyte. When charged, the metal alloy is in the form of a hydride. During discharge, the nickel, in the form of nickel oxyhydroxide, is reduced to nickel hydroxide, while the metal alloy hydride is oxidized to the metal [2].

Two types of intermetallic compounds are contemplated for this type of NiMH battery: (1) the AB₅ class of rare-earth

alloys, such as LaNi₅ and (2) the AB₂ class of alloys, such as ZrV₂ and ZrCr₂. Both alloys consist of a hydride-forming element, such as lanthanum, titanium or zirconium, and a non-hydride-forming element, such as nickel or chromium. The AB₅ class, with a hexagonal CaCu₅ structure, is based on LaNi₅ with some rare-earth substitution for lanthanum to improve the absorption properties and cycle lifetime of the alloy. For example, cerium and neodymium promote the formation of a protective surface film and increase the cycle lifetime. They also increase the equilibrium pressure during charging and discharging [3,4].

New NiMH alloys with high gravimetric energy densities are likely to be developed in response to the demand for inexpensive, durable, high capacity batteries. Similar to the nondestructive techniques used to identify the amount of hydrogen in steel welds [5], magnetic and electronic approaches may be used to determine the amount and state of hydrogen in candidate metal-hydride alloys.

* Corresponding author.

E-mail address: dolson@mines.edu (D.L. Olson).

The objective of this study is to develop new approaches—magnetic measurements and thermopower testing—to determine the amount and type of absorbed hydrogen in these materials and to find new techniques to identify good materials for energy storage applications. These tests can serve as tools for measuring hydrogen in these materials. They complement studies of pressure-composition-temperature (PCT) diagrams using Sieverts' law and hydrogen desorption analysis using gas chromatography.

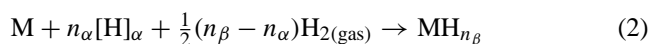
2. Background

2.1. Hydrogen absorption in metal

The absorption of hydrogen in metal can be described by two reactions [6],



and



Here, M represents the metal alloy and MH represents the metal-alloy hydride. To illustrate these reactions, PCT isotherms are used, as shown in Fig. 1. The following is the model proposed in this paper: Initially, atomic hydrogen enters the metal as *soluble* hydrogen, sometimes referred to as *protonic* hydrogen, [H], as shown in reaction (1). (The term “soluble” is preferred to “diffusible” because mobility and kinetics are not addressed.) This behavior is a single-phase reaction, and its range in Fig. 1 is denoted by a single α phase. As the soluble hydrogen in the metal increases, it enters interstitial octahedral and tetrahedral sites to form the metal hydride [6], shown in reaction (2). Hydrogen that is not desorbed at low temperature is denoted in this paper as *bound* hydrogen. Reaction (2) is a two-phase reaction, shown in Fig. 1 as the $\alpha + \beta$ region. When the hydrogen content is large enough, only bound hydrogen will exist as the β phase. The symbols α and β are used, respectively, for the metal with soluble (protonic) hydrogen and the hydride,

which is one of the forms of bound hydrogen. In (2), n_{α} and n_{β} are the ratios of hydrogen to metal atoms for the α and β phases.

The first hydrogen to enter a transition-metal-rich solid solution—at least those rich in transition metal elements to the right of titanium in the periodic table—has a positive heat of mixing. This positive heat of solution suggests that energy is required to move an electron from the hydrogen atom to the electronic band structure. The result is soluble (protonic) hydrogen in the lattice. The phase that exhibits this electronic behavior is the α phase. It obeys Sieverts' law for the solubility of hydrogen gas into a metal or alloy. Models in which interstitial hydrogen atoms contribute their electrons to the metal d-band are often referred to as the “proton” and the “screened proton” models [7,8]. Palladium hydride is an archetypal example.

As the hydrogen activity (and content) increases in the solid solution, the heat of mixing goes negative for these transition-metal-rich alloys. This negative value thermodynamically describes a lowering of energy by the shared (covalent) or transferred (ionic) electron to the hydrogen atom, resulting, to some degree, in a bound hydrogen atom. The more negative the value of the heat of mixing, the more irreversible is the nature of the bound hydrogen. This β phase is characterized by hydrogen as an electron acceptor; it promotes negative hydrogen ion localization to the positive core ion, resulting in hydride formation. Elements of the periodic table to the left of titanium and the lanthanides and actinides probably never exhibit a positive heat of mixing no matter what the hydrogen content is. Hydrogen, which has a small negative heat of mixing, statistically can exhibit soluble hydrogen characteristics at the lower temperatures because its activation energy barrier (mobility energy plus binding energy) may not totally hinder transport.

Fig. 1 shows that the equilibrium pressure increases with temperature, indicating that hydride formation is an exothermic reaction. During desorption, the reverse of reactions (1) and (2) apply. A good intermetallic hydride for battery applications should easily absorb and desorb hydrogen and provide energy at ambient temperatures.

2.2. Effect of electronic structure on absorption of hydrogen

Changing the Fermi energy affects the chemical potential of soluble (protonic) hydrogen in metals. The effect of hydrogen absorption on the electronic structure was reviewed by Gelatt [7], applying a simplified band model as shown in Fig. 2.

Fig. 2 schematically illustrates the electron distribution for three cases [7]. Fig. 2a is the electronic distribution for a transition metal or alloy with no absorbed hydrogen. Fig. 2b is for the metal with electron donation from absorbed hydrogen, where the electrons go primarily into the d-band. Fig. 2c illustrates donations to the d-band, as well as some electrons becoming localized to the hydride bonding band, consuming electrons from the s-band and the p-band and

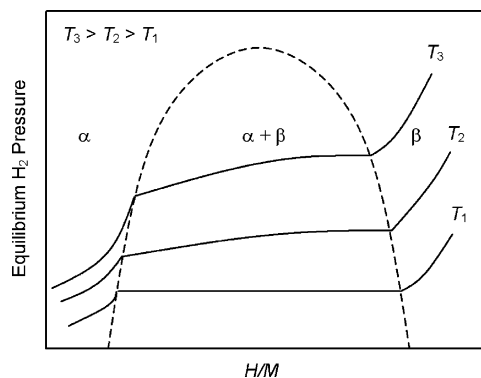


Fig. 1. Generalized PCT isotherms for hydrogen absorption, after Speiser [9] and Bernauer et al. [10].

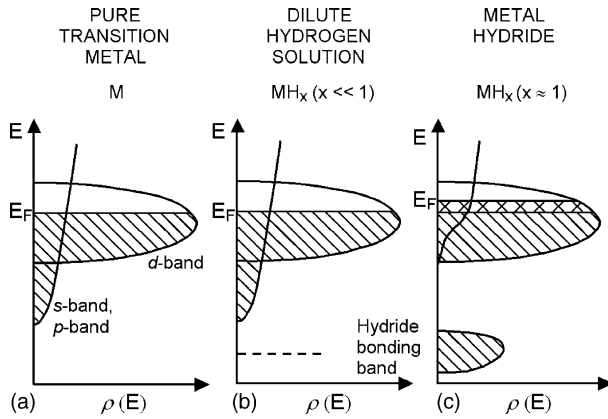


Fig. 2. Electronic structure of hydrides, after Gelatt [7].

causing the formation of a metal hydride. This behavior is the desired characteristic of a hydrogen storage electrode for a reversible battery.

The relationship between hydrogen absorption and the electronic chemical potential was proposed by Yasuda and Brodowsky [11]. They showed that the equilibrium partial pressure of hydrogen P_{H_2} at a given temperature T could be determined by

$$\frac{1}{2} \ln P_{H_2} = \frac{\ln K n_H}{(2/3) - n_H} + \frac{\mu_{elec}}{RT} + n_H \frac{W}{RT} \quad (3)$$

where K is the thermodynamic equilibrium constant, n_H the hydrogen concentration, μ_{elec} the electronic chemical potential, and W the elastic energy of attraction responsible for the two-phase formation.

Another model for the electronic effect on hydrogen absorption in metals was proposed by Bernauer et al. [10]. This model pointed out that hydrogen absorption for the cubic and hexagonal transition-metal alloys depends only on the average number of d-electrons, which is described by

$$\frac{H}{M} = 5 - DEC \quad (4)$$

where H is the number of stored hydrogen atoms, M the number of metal atoms, and DEC is the average number of d-electrons (before hydrogen is introduced), which is calculated from

$$DEC = \frac{\text{sum of d-electrons}}{\text{number of metal atoms}} \quad (5)$$

According to this model, soluble hydrogen will be stored until the 3d-band is half-full; after that, absorbed hydrogen will cause hydride formation.

By modifying this model, as proposed in the present paper, the hydrogen absorption for rare-earth transition-metals may be expressed by

$$\frac{H}{M} = X(5 - DEC) + Y(7 - FEC) \quad (6)$$

where X is the total atomic fraction of elements that provide d-orbitals, Y the total atomic fraction of elements that pro-

vide f-orbitals, and FEC the average number of f-electrons, which is determined by

$$FEC = \frac{\text{sum of f-electrons}}{\text{number of f-metal atoms}} \quad (7)$$

Eq. (4) can be rearranged to

$$\frac{H}{M} = 5X + 7Y - DFEC, \quad (8)$$

$$DFEC = \sum e_{di} X_i + \sum e_{fi} Y_i, \quad (9)$$

where e_{di} and e_{fi} are the number of d- and f-electrons given by element i , and X_i and Y_i are the atomic fractions of element i that provides d- and f-electrons.

Based on Eqs. (4) and (5) and a simple band-filling model of magnetism—in which electrons occupy orbitals to maximize total spin angular momentum, subject to the Pauli exclusion principle—absorbed hydrogen will change the magnetic moment of an alloy (Hund's rule). Conversely, the amount of absorbed hydrogen may be gauged by the change in magnetic moment after hydrogen charging. Examples of how hydrogen content reduces the magnetic moment of the transition metal in rare-earth transition-metal alloys were reported by Buschow and Sherwood [12].

Fig. 3 shows how the known equilibrium pressures of $\text{LaNi}_{5-x}\text{Al}_x$ alloys at $H/M = 0.5$, based on data from Wang and Suda [13], are actually related to the alloys' calculated DEC numbers. The choice $H/M = 0.5$ places an alloy at about the middle of the plateau of the PCT diagram in Fig. 1. The designation LaNi_5 , for example, at $H/M = 0.5$ corresponds to LaNi_5H_3 . (At $H/M = 1$ it would correspond to LaNi_5H_6 .) In this system, with Ni being on the right side of the periodic table, the ability to absorb hydrogen is inversely proportional to the equilibrium hydrogen pressure; this pressure will be proportional to the DEC and DFEC numbers, which are functions of H/M .

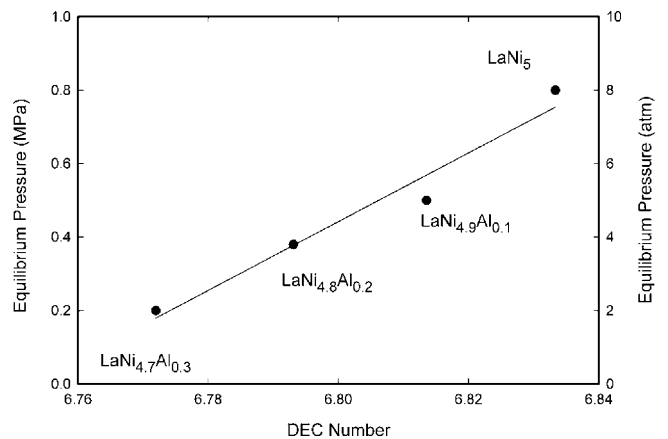


Fig. 3. Relation between DEC number and equilibrium pressure at $H/M = 0.5$ for $\text{LaNi}_{5-x}\text{Al}_x$ hydrides, based on data from Wang and Suda [13]. This is a reflection of the change in lattice constant. Since La has no f-electrons, DFEC number equals DEC number.

Table 1
Alloy compositions in atomic percent and calculated B/A ratio

Alloy	Type	A						B						B/A ratio	
		La	Ce	Nd	Mg	Zr	Ti	Ni	Mn	Co	Al	Fe	Cr		V
1 ^{a,b}	AB ₅	7.7	8.1		0.6			71.2	12.0		0.4				5.1
2 ^{c,d}	AB ₅	8.3		8.3				59.2	6.7	12.5	5.0				5.0
3 ^{a,b}	AB ₂					19.0	16.7	29.2	16.9				7.9	10.4	1.8
4 ^{a,d}	AB ₂					29.5	4.0					47.3	19.3		2.0

^a Composition as verified by energy dispersive spectroscopy.

^b Alloy prepared by Ovonic Battery Company, cathodically charged.

^c Target composition, as fabricated.

^d Alloy prepared by Brookhaven National Laboratory, gas-phase charged.

3. Experimental methods

3.1. Sample preparation

Samples as received were pieces on the order of 1–2 mm in size. Table 1 shows the compositions as measured with an energy dispersive spectrometer attached to a scanning electron microscope or, in the case of one alloy, the target composition based on the masses of the elements used in fabrication. Alloys 1 and 3 were baked in an argon environment at 400 °C for 3 h before being charged with hydrogen gas. Alloys were either cathodically charged (Alloys 1 and 3) or gas-phase charged using the PCT technique (Alloys 2 and 4). Gas-phase charging involved six activation (hydrogenation) cycles of full charge and discharge. It is well known that activation cycling reduces alloy particle size. After six cycles, the gas-phase charged alloys had particle sizes of 2–5 μm.

A total of six activation cycles is not expected to cause significant precipitation of nickel or iron at the surface, an effect reported by Stucki and Schlapbach [14] for large numbers of activation cycles. Although any such precipitates would increase the overall magnetization, they would not influence the effect of hydrogen content on magnetization, which is reported here for a given activation state. Of the alloys studied, only gas phase charged Alloys 2 and 4 may have nickel or iron precipitates. After charging, Alloys 2 and 4 were “poisoned” by carbon monoxide to prevent hydrogen from diffusing out at room temperature [15].

3.2. Hydrogen analysis

Thermal desorption analysis (TDA) was used to determine the amount and specific site location of hydrogen absorbed by all alloys [16]. To desorb hydrogen, the charged materials were heated from room temperature to 650 °C at a rate of about 4 °C/min in an argon atmosphere. The hydrogen desorption curve was measured on a companion sample. During heating, the amount of desorbed hydrogen was measured by gas chromatography by calculating the area under the desorption curve. To prepare samples for magnetic and thermoelectric coefficient measurements, the companion charged sample was heated. The sample for measure-

ment was removed from the system at different temperatures determined from the hydrogen desorption curve, and quenched in dry ice. Details of the technique are given by Wunderlich [17]. In addition, the hydrogen content of some alloys (Alloys 2 and 4) was determined by PCT isotherms in a calibrated-volume system.

In a plot of hydrogen desorption as a function of temperature, two major hydrogen evolution peaks are evident in different temperature ranges, as described in the next section. A peak at high temperature, about 650 °C, is from bound hydrogen that is not desorbed from interstitial sites at low temperature. A hydrogen release peak at lower temperature, about 200 °C, is from soluble (protonic) hydrogen. In this work, a direct correlation is obtained between the amount of soluble hydrogen and the ferromagnetic properties of the specimens.

Another technique was used to measure small amounts of absorbed hydrogen. In this system, the charged sample in powder form was loaded in a very high temperature chamber at 2500 °C. The released hydrogen gas was carried by ultra-high purity argon through a calibrated thermal conductivity detector (TCD). The amount of hydrogen was recorded in parts per million and later converted to hydrogen per formula unit.

3.3. Magnetic measurements

The objective of the magnetic measurements was to determine the effect of absorbed hydrogen on saturation magnetization, magnetic susceptibility, and magnetic hysteresis. The absorbed hydrogen in transition-metal alloys is present as metal hydride and soluble hydrogen atoms [7]. Each free hydrogen atom carries one electron, which can increase or decrease the magnetic moment of the alloys. If the electrons from hydrogen have the same spin as the majority of the electrons in the d-band in the alloy, the magnetic moment will increase. The magnetic moment decreases when the electrons have the opposite spin. Expansion of the crystal lattice, of order 6%, with increasing hydrogen content may also affect magnetic properties [18]; however, such effects are not modeled in the present work.

Magnetization hysteresis loops were measured with a transverse-field vibrating-sample magnetometer at room

temperature in maximum applied fields of 0.6 T. Magnetization was computed as magnetic moment per unit mass of metal, not including hydrogen, and expressed in units of $\text{A m}^2/\text{kg}$ (equivalent to emu/g). The exclusion of hydrogen causes an uncertainty of 0.1–2% in the mass determination. Uncertainty arising from random effects is estimated to be on the order of the size of the data points on the graphs. Uncertainty arising from systematic effects is estimated to be less than 5% of the reported values.

3.4. Thermopower measurements

The objective of this measurement was to study the effect of absorbed hydrogen on the thermoelectric power as expressed by the Seebeck coefficient [19,20]. The thermopower, an intrinsic property of a material, characterizes the electronic density of states at the Fermi level: the amount of electric charge and the type of charge carrier. (The presence of hydrogen in transition-metal alloys alternatively has been detected by changes in electrical resistivity [21,22].)

A simple and flexible experimental apparatus (Fig. 4) consists of two massive copper blocks maintained at different temperatures measured with thermocouples mounted inside the blocks. The powder sample is enclosed in a plastic tube between the ends of the copper blocks. The potential difference is measured across the two copper probes. Usually, good electrical and thermal contacts are needed between the sample surface and probes. For these powder measurements, repeatability was 10–15%. Thermopower measurements on powder are a new advance in materials characterization.

The absolute thermopower (Seebeck coefficient S_a) of the alloy material can be determined as

$$S_a = \frac{\Delta V}{\Delta T} + S_{\text{Cu}}, \quad (10)$$

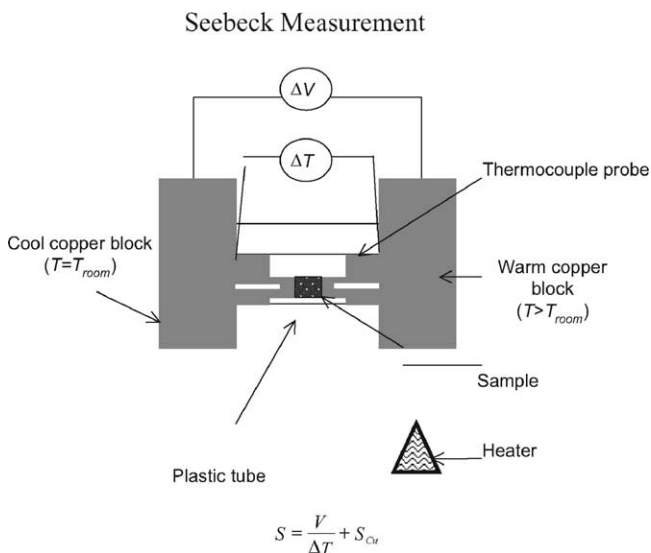


Fig. 4. Sketch of the thermoprobe Seebeck measurement.

where ΔV is the voltage difference measured between probes, ΔT the temperature difference, and S_{Cu} the well-known Seebeck coefficient for copper, $1.83 \mu\text{V/K}$ at 300 K [23]. One of the blocks was maintained at room temperature and the other around 10°C higher.

In a similar arrangement for bulk materials, the correlation of the Seebeck coefficient to alloy hydrogen content allows a probe with two surface contacts to make a nondestructive hydrogen analysis of welds in fabricated structures [5].

4. Results and discussion

Table 1 shows the chemical composition in atomic percent of the alloys tested in this work. The estimated uncertainty is 5% times the atomic percentages given in the table. The actual B/A atomic ratios are given in the last column. Table 2 shows the composition in atomic ratio, which is how the data plots are labeled in this paper.

4.1. AB_5 alloys

Alloy 1, $(\text{La-Ce})(\text{Ni-Mn})_5$, and Alloy 2, $(\text{La-Nd})(\text{Ni-Co-Mn})_5$, are of type AB_5 . Figs. 5 and 6 show the hydrogen desorption curves determined by gas chromatography. The initial hydrogen charges were 2.23 and 1.83 per formula unit. Desorption of soluble (protonic) hydrogen, which most likely is present in the α phase, occurs at about 220 and 110°C , respectively. The release of bound hydrogen at temperatures above 600°C is indicative of hydride decomposition in Alloy 1. Both the low-temperature desorption and the absence of bound hydrogen would make Alloy 2 a good candidate for battery applications.

The magnetization curves and the technical saturation magnetization as a function of hydrogen contents for Alloy 1 are shown in Figs. 7 and 8. (To convert magnetic field from units of tesla to units of ampere per meter, multiply by

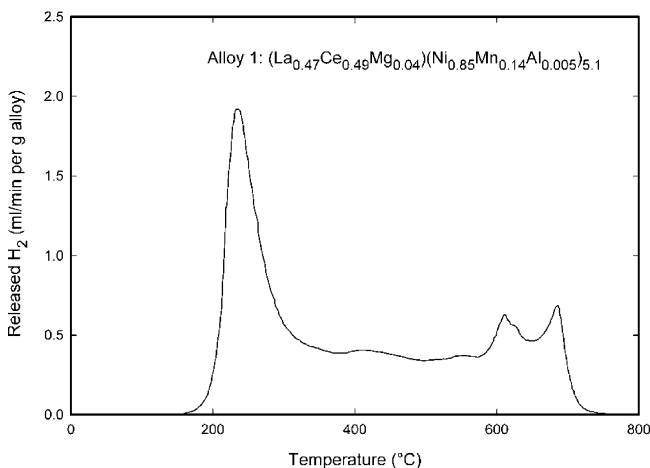


Fig. 5. Hydrogen desorption curve for Alloy 1 hydride as a function of temperature.

Table 2
Alloy compositions in formula units

Alloy	Formula	A						B						
		La	Ce	Nd	Mg	Zr	Ti	Ni	Mn	Co	Al	Fe	Cr	V
1	AB _{5.1}	0.47	0.49		0.04			0.85	0.14		0.005			
2	AB _{5.0}	0.50		0.50				0.71	0.08	0.15	0.06			
3	AB _{1.8}					0.53	0.47	0.45	0.26				0.12	0.16
4	AB _{2.0}					0.88	0.12					0.71	0.29	

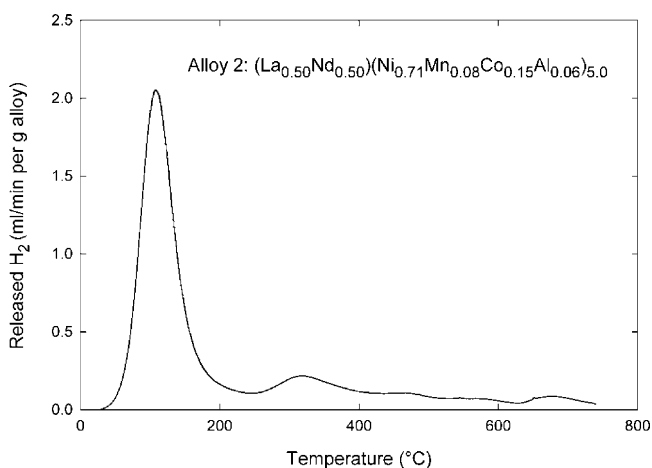


Fig. 6. Hydrogen desorption curve for Alloy 2 hydride as a function of temperature.

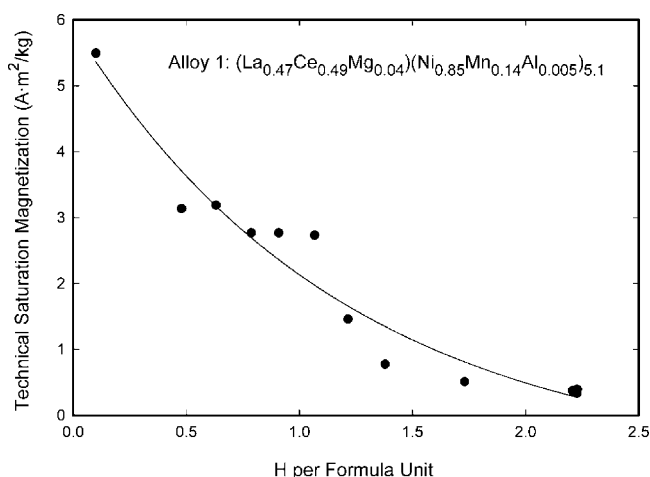


Fig. 8. Technical saturation magnetization as a function of hydrogen content for Alloy 1.

$10^7/4\pi$. To convert magnetic field from SI units of tesla to CGS units of gauss, multiply by 10^4 .) The technical saturation magnetization is the magnetization axis intercept of a line fitted to the high field part of the curve of magnetization as a function of field. An increase in soluble hydrogen decreases the magnetization of Alloy 1. The DFEC number for Alloy 1 is calculated as 6.51, whereas the number of electrons required to half-fill the d- and f-bands is 5.47.

The reduction of magnetic moment results from electrons donated by the hydrogen atoms pairing with the unpaired electrons in the host metal.

For Alloy 2, as a function of hydrogen content, Fig. 9 shows the magnetization curves and Fig. 10 shows the initial susceptibility near zero field (not corrected for demagnetizing factor) and high field susceptibility. (To convert from SI units of m^3/kg to CGS units of cm^3/g , multiply by $1000/4\pi$.) Initially, the susceptibilities decrease as hydrogen increases,

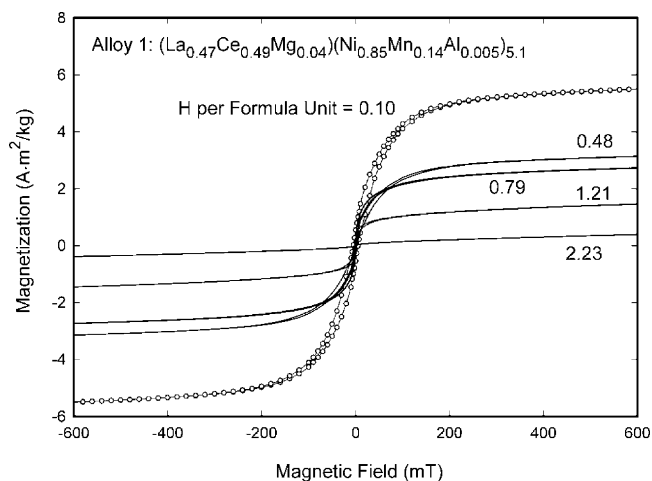


Fig. 7. Magnetization versus field for Alloy 1. As hydrogen content H increases, magnetization and hysteresis decrease.

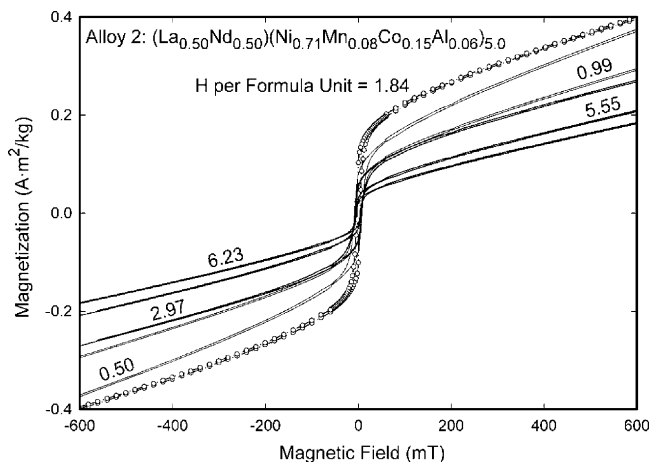


Fig. 9. Magnetization versus field as a function of hydrogen content for Alloy 2.

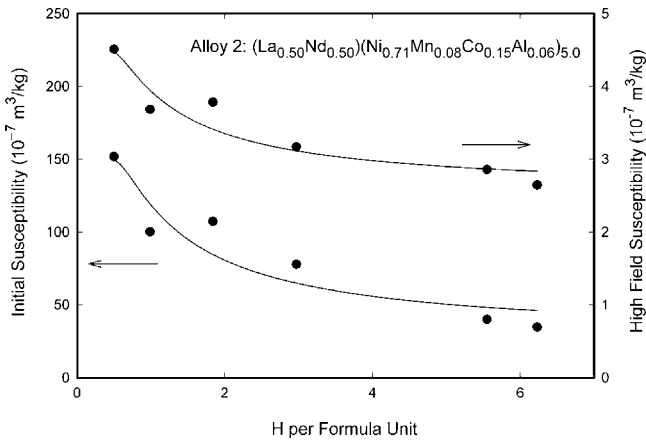


Fig. 10. Initial and high field susceptibilities as functions of hydrogen content in Alloy 2.

but then increase after the ratio of hydrogen to metal is 1. The susceptibilities decrease again when the hydrogen-to-metal ratio is greater than 2. The computed DFEC number of Alloy 2 is 6.48, also above the number of electrons to half-fill the d- and f-bands, 5.33. Therefore, a decrease in susceptibility is expected. The difference in the magnetic behavior between Alloys 1 and 2 may depend on the details of the actual band structure of the alloys.

The room temperature Seebeck coefficients and PCT isotherm of Alloy 2 are shown in Fig. 11. The Seebeck coefficient of this alloy increases with an increase in hydrogen content until it reaches a plateau region, in which the two-phase reaction occurs, at a hydrogen content per formula unit of about 1, and increases again at the transition from the two-phase region to the single-phase hydride region. In the first stage, each hydrogen atom provides an electron to the host material, which changes the Fermi level of the material. In the plateau region, lattice expansion occurs as the bound hydrogen forms a hydride, and the added electrons from the hydrogen have less of an effect on the Fermi energy.

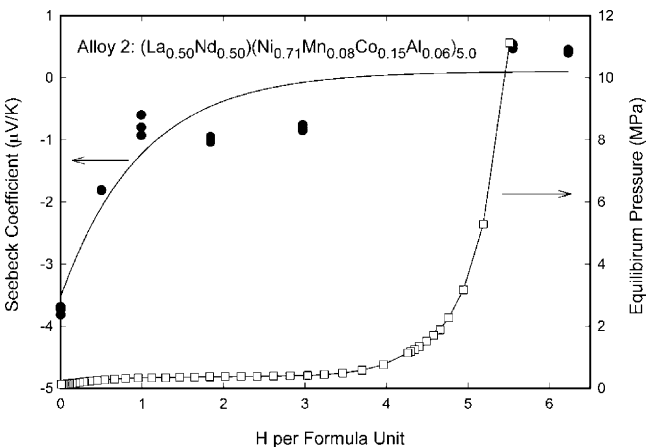


Fig. 11. The thermoelectric power (Seebeck coefficient) at 25 °C and the PCT diagram at 75 °C of Alloy 2 as functions of hydrogen content.

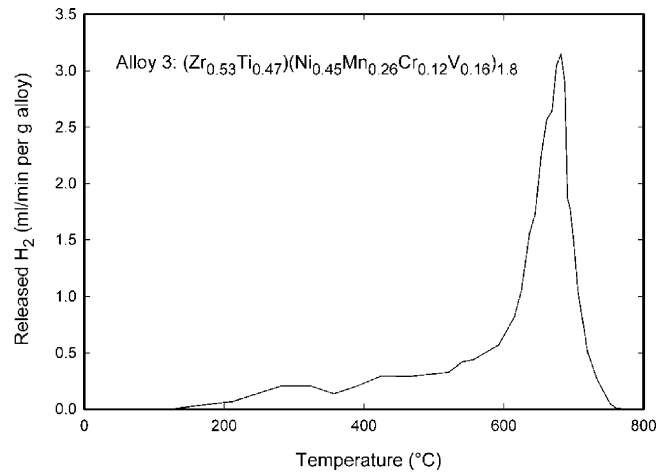


Fig. 12. Hydrogen desorption curve for Alloy 3 hydride indicating the release of hydrogen only at a high temperature of about 680 °C.

4.2. AB₂ alloys

Unlike Alloys 1 and 2, Alloy 3, which is AB₂ type, has a main hydrogen desorption peak at 680 °C, as shown in Fig. 12. The initial hydrogen charge was 0.91 per formula unit. This result indicates that most of the hydrogen in Alloy 3 is stored as bound hydrogen, with a little amount of soluble hydrogen indicated by peaks at lower temperature. In contrast, the hydrogen desorption curve of Alloy 4, shown in Fig. 13, shows a main peak at 220 °C, which is in the soluble hydrogen range. The initial hydrogen charge was 4.10 per formula unit. The relatively large amount of released hydrogen per gram of Alloy 4 is due to its low molecular weight and its large initial hydrogen content from gas-phase charging.

Magnetization curves and the initial susceptibilities of Alloys 3 and 4 are shown in Figs. 14–17. Both the change in hydrogen content and the change in susceptibility of Alloy 3 are relatively small compared with Alloy 4. The calculated

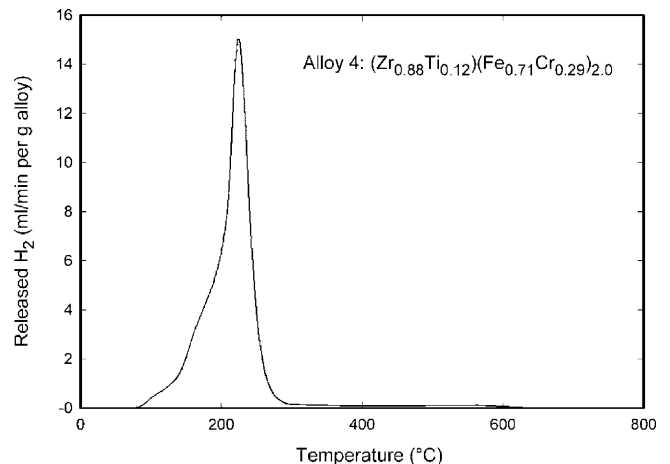


Fig. 13. Hydrogen desorption curve for Alloy 4 hydride indicating the release of hydrogen at 220 °C.

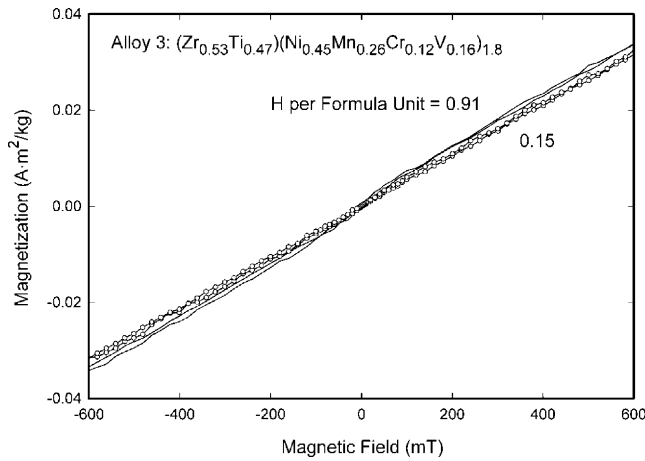


Fig. 14. Magnetization versus applied field as a function of hydrogen content in Alloy 3.

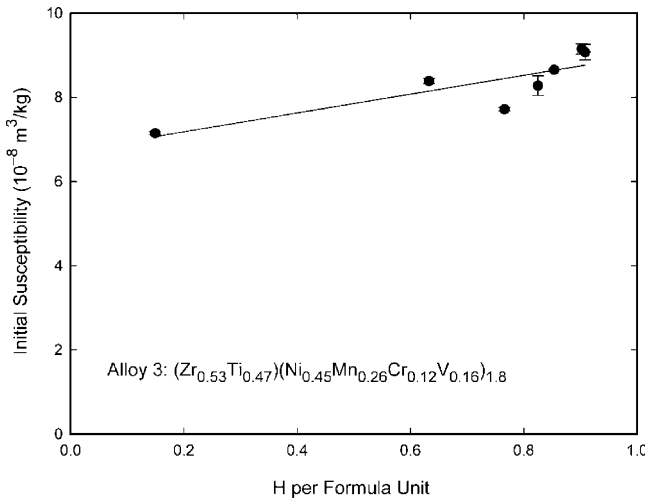


Fig. 15. Initial susceptibility of Alloy 3 indicating no significant change in susceptibility as hydrogen content increases. Error bars represent the random uncertainty in the magnetization curves.

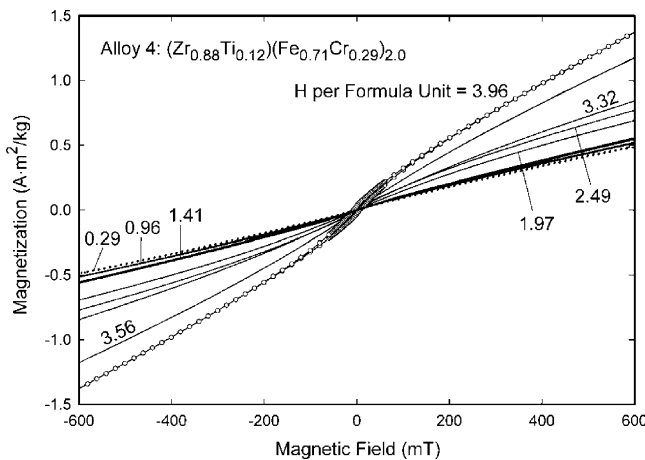


Fig. 16. Magnetization versus applied field as a function of hydrogen content in Alloy 4.

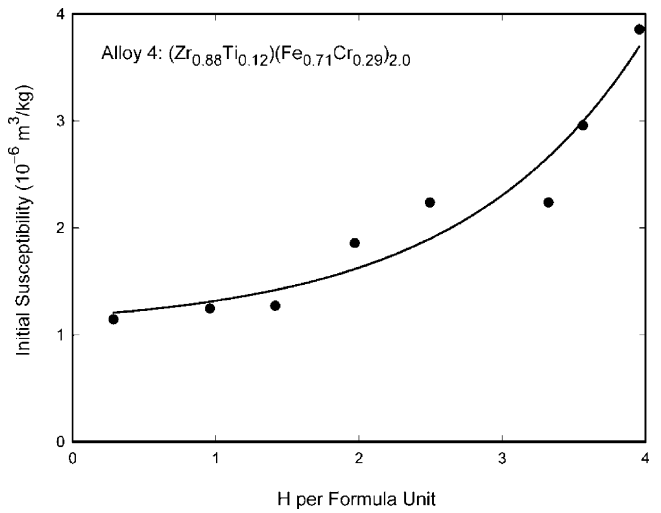


Fig. 17. Initial susceptibility of Alloy 4 indicating an increase of susceptibility as hydrogen content increases.

DEC number of Alloy 3 is 4.23, which is less than the number of electrons required to occupy a half-band. Therefore, if hydrogen gives additional electrons only to the d-band, the initial susceptibility should increase with the amount of hydrogen. However, the initial susceptibility curve for Alloy 3 shows that hydrogen has almost no effect on the initial susceptibility (Fig. 15). Since Fig. 12 shows that Alloy 3 holds hydrogen as *bound* hydrogen, the transfer of an electron from the host metal and the formation of the hydride bonding band may dominate and not affect the magnetic moment. (A reduction of the Fermi energy during hydride formation was reported for LaNi₅ [24].)

On the other hand, the initial susceptibility for Alloy 4 *increases* with soluble hydrogen (Fig. 17). The computed DEC number of Alloy 4 is 4.27, also less than the number of electrons required to occupy a half-band. Thus, it seems that electrons from soluble hydrogen enter the conduction band and increase the magnetic susceptibility.

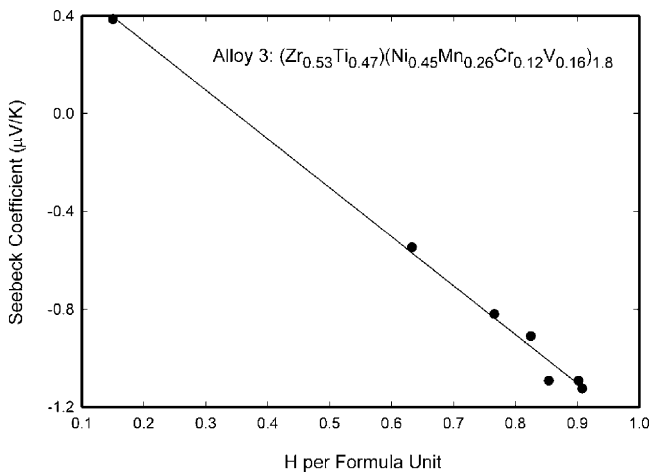


Fig. 18. Room temperature Seebeck coefficient as a function of hydrogen content in Alloy 3.

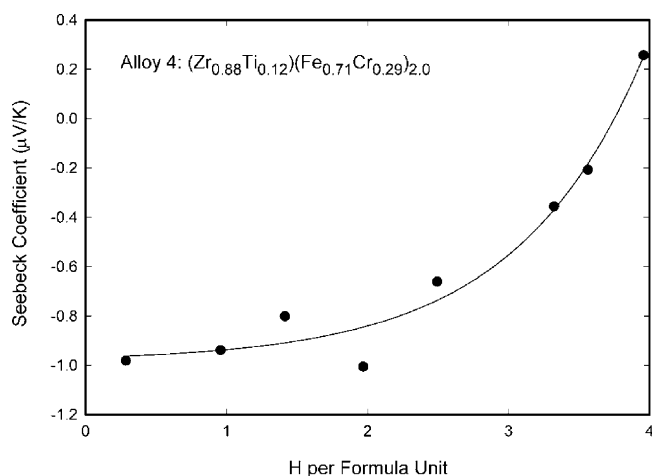


Fig. 19. Room temperature Seebeck coefficient as a function of hydrogen content in Alloy 4.

For AB₂ alloys, the room-temperature Seebeck coefficient of Alloy 3 decreases as hydrogen content increases as shown in Fig. 18. Conversely, the thermoelectric power of Alloy 4 increases with hydrogen content as shown in Fig. 19. The markedly different dependence of the Seebeck coefficient on hydrogen content is likely due to the different forms of hydrogen (bound hydrogen for Alloy 3 and soluble hydrogen for Alloy 4) in the alloys.

5. Conclusions

Measurements of magnetization and thermopower may be used as tools for the selection of materials for their hydrogen storage capabilities and to indicate whether absorbed hydrogen is bound or soluble.

Four candidate NiMH battery materials were evaluated to determine the role of soluble and bound hydrogen in the alloys on magnetic and Seebeck coefficient measurements. The soluble and bound hydrogen are identified by the released hydrogen peaks in the hydrogen desorption curve. The lower temperature peak, near 200 °C, indicates the presence of soluble hydrogen and the high temperature peak, near 600 °C, indicates bound hydrogen.

Absorbed hydrogen either decreases or increases the magnetization depending on whether the d- and f-bands are more or less than half-filled and whether hydrogen is soluble or bound.

- An increase in *soluble* (protonic) hydrogen content *decreases* the magnetization in AB₅ Alloys 1 and 2, which have *more* than half-filled bands.
- An increase in *soluble* (protonic) hydrogen content *increases* the magnetization in AB₂ Alloy 4, which has *less* than half-filled bands.
- An increase in *bound* hydrogen content has almost *no effect* on the magnetization in AB₂ Alloy 3, which has *less* than half-filled bands.

The effect of absorbed hydrogen on the thermoelectric properties of the materials depends on the types of hydrogen stored and the electronic states of the materials before absorption. The thermoelectric power of Alloy 2 shows that the trend of the Seebeck coefficient recapitulates the shape of the hydrogen PCT isotherm. However, the thermoelectric power of AB₂ Alloys 3 and 4 are more affected by the type of absorbed hydrogen. Bound hydrogen reduces the Seebeck coefficient of Alloy 3 and soluble hydrogen has the opposite effect on Alloy 4.

Acknowledgements

The authors thank the National Institute of Standards and Technology (NIST) Advanced Technology Program and the US Army Research Office for financial support. For providing the alloy samples, thanks are due to the Ovonic Battery Company, Troy, Michigan (Alloys 1 and 3), and John Johnson, Brookhaven National Laboratory, Upton, New York (Alloys 2 and 4). Dr. Johnson also provided helpful information on the preparation, characterization and hydrogenation of AB₅ compounds.

References

- [1] K.H.J. Buschow, P.C.P. Bouten, A.R. Miedema, Rep. Prog. Phys. 45 (1982) 937–1039.
- [2] D. Linden, Handbook of Batteries, second ed., McGraw-Hill, New York, 1995, pp. 33.1–33.29.
- [3] J. Chen, S.X. Dou, H.K. Liu, J. Power Sources 63 (1996) 267–270.
- [4] G.D. Adzic, J.R. Johnson, J.J. Reilly, J. McBreen, S. Mukerjee, M.P. Sridhar Kumar, W. Zhang, S. Srinivasan, J. Electrochem. Soc. 142 (1995) 3429–3433.
- [5] D.L. Olson, B. Mishra, R.D. Smith, S. Niyomsoan, P. Termsuksawad, Y.D. Park, V.I. Kaydanov, Z. Gavra, R.B. Goldfarb, in: J.E. Indacochea, J.N. DuPont, T.J. Lienert, W. Tillmann, M. Singh (Eds.), Joining of Advanced and Specialty Materials IV, ASM International, Materials Park, OH, 2002, pp. 118–124.
- [6] T.B. Flanagan, W. A. Oates, in: L. Schlapbach (Ed.), Hydrogen in Intermetallic Compounds. Part I. Electronic, Thermodynamic, and Crystallographic Properties, Preparation, Springer, Berlin, 1988, pp. 49–85.
- [7] C.D. Gelatt, in: L.H. Bennett (Ed.), Theory of Alloy Phase Formation, Metallurgical Society, AIME, Warrendale, PA, 1980, pp. 451–469.
- [8] W. Pepperhoff, M. Acet, Constitution and Magnetism of Iron and Its Alloys, Springer, Berlin, 2001, pp. 172–181.
- [9] R. Speiser, in: W.M. Mueller, J.P. Blackledge, G.G. Libowitz (Eds.), Metal Hydrides, Academic, NY, 1968, pp. 67–70.
- [10] O. Bernauer, J. Töpler, D. Noréus, R. Hempelmann, D. Richter, Int. J. Hydrogen Energy 14 (1989) 187–200.
- [11] K. Yasuda, H. Brodowsky, J. Alloys Compd. 231 (1995) 454–459.
- [12] K.H.J. Buschow, R.C. Sherwood, J. Appl. Phys. 49 (1978) 1480–1485.
- [13] X.L. Wang, S. Suda, J. Alloys Compd. 191 (1993) 5–7.
- [14] F. Stucki, L. Schlapbach, J. Less Common Metal 74 (1980) 143–151.
- [15] J.R. Johnson, J.J. Reilly, Inorg. Chem. 17 (1978) 3103–3108.

- [16] I. Maroef, D.L. Olson, M. Eberhart, G.R. Edwards, *Int. Mater. Rev.* 47 (2002) 191–223.
- [17] B. Wunderlich, *Thermal Analysis*, Academic, San Diego, CA, 1990, pp. 123–169.
- [18] B.D. Cullity, *Introduction to Magnetic Materials*, Addison-Wesley, Reading, MA, 1972, p. 134.
- [19] A.W. Szafranski, *J. Alloys Compd.* 316 (2001) 82–89.
- [20] B.V. Sharov, O.A. Smirnov, *Atom. Energy* 89 (2000) 937–938.
- [21] F. Ishikawa, H. Tega, I. Yamamoto, M. Yamaguchi, *J. Alloys Compd.* 231 (1995) 182–187.
- [22] K. Azumi, Y. Asada, T. Ueno, M. Seo, T. Mizuno, *J. Electrochem. Soc.* 149 (2002) B422–B427.
- [23] D.M. Rowe (Ed.), *CRC Handbook of Thermoelectrics*, CRC Press, Boca Raton, FL, 1995, p. 390.
- [24] H. Nakamura, D. Nguyen-Manh, D.G. Pettifor, *J. Alloys Compd.* 281 (1998) 81–91.